L- and *M*-shell x-ray production cross sections of Nd, Gd, Ho, Yb, Au, and Pb by 25-MeV carbon and 32-MeV oxygen ions

M. C. Andrews,* F. D. McDaniel, and J. L. Duggan
Department of Physics, North Texas State University, Denton, Texas 76203

P. D. Miller, P. L. Pepmiller, H. F. Krause, and T. M. Rosseel
Physics Division, Oak Ridge National Laboratory, Oak Ridge, Tennessee 37830

L. A. Rayburn
Department of Physics, University of Texas at Arlington, Arlington, Texas 76019

R. Mehta and G. Lapicki
Department of Physics, East Carolina University, Greenville, North Carolina 27858
(Received 27 April 1987)

L- and *M*-shell x-ray production cross sections have been measured for thin solid targets of neodymium, gadolinium, holmium, ytterbium, gold, and lead by 25-MeV $^{12}_{6}C^{q+}$ ($q=4,5,6$) and by 32-MeV $^{16}_{8}O^{q+}$ ($q=5,7,8$). The cross sections were determined from measurements made with thin targets (less than 2.25 $\mu g/cm^2$). For projectiles with one or two *K*-shell vacancies, the target x-ray production cross sections were found to be enhanced over those for projectiles without a *K*-shell vacancy. The sum of direct ionization to the continuum (DI) plus electron capture (EC) to the $L,M,N,\ldots$ shells and EC to the *K* shell of the projectile have been extracted from the data. The results are compared to the predictions of first Born theories, i.e., plane-wave Born approximation for DI and Oppenheimer-Brinkman-Kramers formula of Nikolaev for EC, and to the ECPSSR that accounts for energy loss and Coulomb deflection of the projectile as well as for relativistic and perturbed stationary states of inner-shell electrons.

I. INTRODUCTION

Interest in inner-shell ionization in ion-atom collisions has resulted in major advances both theoretically and experimentally.[1] This information is important in the development of tokamaks,[2] plasma physics,[3] ion implantation,[4] and in particle-induced x-ray emission (PIXE).[5,6] Initially, the majority of the experimental work was done using low-atomic-number ions, primarily protons, to ionize *K*-shell electrons from target atoms.[7] With the development of high-resolution Si(Li) detectors and the increased availability of heavy-ion beams, ionization measurements have been extended to the *L* shell[8,9] and *M* shell.[10]

At the time when advances were being made in the experimental studies, several theories were proposed to describe the dynamics of an ion-atom collision. The plane-wave Born approximation (PWBA),[11,12] the binary-encounter approximation (BEA),[13] and the semiclassical approximation (SCA) (Ref. 14) were successful in describing direct ionization (DI) of the target *K* shell by protons. Later the PWBA was modified[15,16] for low relative velocity effects of enhanced target electron binding and Coulomb deflection which increase with Z_1/Z_2 where Z_1 and Z_2 are the atomic numbers of the projectile and target atoms, respectively.

In addition to DI, electron capture (EC) of target electrons to vacancies in the projectile can play an important part in ionization.[17] The first Born calculations use the PWBA to describe DI and the Oppenheimer-Brinkman-Kramers (OBK) theory[18] as modified by Nikolaev[19] (OBKN) to describe electron capture. Using the perturbed-stationary-states (PSS) approach that was used in DI calculations[20,21] for *K*-shell ionization, Lapicki and Losonsky[22] have developed another approach to EC, also called ECPSSR, where energy loss (E), Coulomb deflection (C), and refinements for target relativistic effects (R) have been taken into account.[23] It has been improved and extended to the *L* and *M* shells by Lapicki and others.[24–28]

In the present paper we report the simultaneous measurement of *L*- and *M*-shell x-ray production for projectiles of 25-MeV $^{12}_{6}C^{q+}$ ($q=4,5,6$) and 32-MeV $^{16}_{8}O^{q+}$ ($q=5,7,8$) incident upon thin (less than 2.25 $\mu g/cm^2$) targets of $_{60}$Nd, $_{64}$Gd, $_{67}$Ho, $_{70}$Yb, $_{79}$Au, and $_{82}$Pb. The purpose of this work was to make independent determinations of the *L*- and *M*-shell x-ray production cross sections and then compare them to predictions of the first Born and ECPSSR theories. Preliminary *L*-shell x-ray production cross sections have been previously reported.[9] These earlier data have been improved by using more refined data analysis techniques as discussed in Sec. II B.

II. EXPERIMENTAL DETAILS

A. Target preparation

The target foils used in this experiment were made at North Texas State University (NTSU) by vacuum evaporation of the various elements onto (5–20 $\mu g/cm^2$) carbon backings. Each set of target foils ranged from approximately 0.5 to 100 $\mu g/cm^2$. Targets with thicknesses less than 2.25 $\mu g/cm^2$ were used for cross-section determinations while the thicker targets were used to study target thickness dependence and to obtain initial fit parameters during data analysis (cf. Sec. II B).

Usually target contamination is dominated by low-Z elements which have x rays at the same energies as the soft M-shell x rays. Steps taken during target preparation to reduce the presence of these contaminants are described elsewhere.[29] They consisted primarily of repeated bathing of the carbon foils in weak solutions of warm (40–60 °C) acetone. The foils, after mounting on target frames, were analyzed to ensure that they were relatively contaminent-free. The 2.5-MV Van de Graaff accelerator at NTSU was used to provide protons for target analysis by proton-induced x-ray emission.

While target contamination was being monitored, Rutherford ion backscattering was used to determine the target thicknesses. The scattered-particle yields were measured with a Si surface barrier detector placed at 150° relative to the incident ion beam direction. These yields, the theoretical Rutherford scattering cross sections, and the number of incident protons were used to determine the target thicknesses. The resulting thicknesses have a total uncertainty of ±7% due to uncertainties in source calibration (3%), solid angle (2%), ion energy (3%), and counting statistics (5%).

B. X-ray cross-section measurements

The ions used in this experiment were obtained from the 6.5-MV EN Tandem Van de Graaff accelerator at the Oak Ridge National Laboratory. Primary beams of C^{4+} and O^{5+} were produced at energies of 25 and 32 MeV, respectively. Each beam was then electromagnetically analyzed for the desired charge state before being focused and directed into the target chamber. Prior to entry into the target chamber, the beam was collimated to 6.4-mm diameter. A pair of carbon collimators, 12.5- and 5-cm in front of the target holder, further narrowed the beam to 3.2-mm diameter. The central target holder was oriented at 45° relative to the incident beam direction. An Ortec Si(Li) detector was positioned at 90° relative to the incident beam direction and in such a manner as to view the incident side of the target.

To obtain the best available values for the detector efficiency, a technique by Lennard and Phillips[30] was employed which suggested using theoretical x-ray cross sections in a "reverse" calculation. Bombardment of several thin targets of low-Z elements ($_{13}$Al, $_{14}$Si, $_{15}$P, $_{17}$Cl, and $_{19}$K) provided K-shell x rays. The Rutherford scattered-particle yields of the projectile were collected simultaneously and were used to normalize the x-ray yields. This information, along with the theoretical x-ray production cross sections from the ECPSSR and the fluorescence yields and transition rates of McGuire[31] were used to determine the Si(Li) detector efficiency at points below 3.3 keV.[10,32] For energies above 3.3 keV, calibrated sources of ^{55}Fe, ^{57}Co, and ^{241}Am provided x rays of known intensities from which the efficiencies were determined. The theoretical efficiency curve of the detector above 3.3 keV was obtained by calculating the x-ray attenuation in the Be entrance window, the Si dead layer, and the Au contact layer.[10] This curve was then normalized to the data points for the radioactive sources, and the efficiencies corresponding to L- and M-shell x-ray energies were determined.

While x rays were being counted by the Si(Li) detector, Rutherford scattered particles were simultaneously being collected by a solid-state charged-particle detector positioned at either 45° or 135° relative to the incident beam direction. These results were used to find the product of the number of ions incident upon each target and the target thickness which was used to normalize the x-ray yields.

Each set of spectra, containing L- and M-shell x rays and Rutherford yields, was processed with a common configuration of signal processing equipment and then stored on the ORNL computer facilities for later recall and analysis. This equipment consisted of a PDP 11/45 computer and a Hewlett Packard CRT with light-pen capabilities. Throughout the experiment the x-ray yields were monitored for consistency. Each spectrum was displayed on the CRT and a background was drawn in by hand. The resulting yields along with initial estimates of the detector efficiency were used to monitor the experimental results as they were generated. This control was especially useful because of the long counting times required to obtain acceptable yields from the thinnest targets. After completing the experiment, an Ortec 7050 Data Acquisition and Analysis System with peak-fitting capabilities was used to analyze the relatively clean L-shell spectra. A least-squares-fitting routine (FACELIFT) (Ref. 33) gave complete analysis of each M-shell spectrum. This program was capable of fitting multiple Gaussian peaks on a linear background. A typical M-shell x-ray spectrum and the results of a fit are illustrated in Fig. 1. After initially reporting the L-shell results[9] obtained with the Ortec system, the data were analyzed using the FACELIFT procedure. The previously extracted data obtained by the light-pen fit differed very little from that obtained by the FACELIFT procedure.

The fitting procedure for the M-shell targets consisted of using spectra of thicker targets ($\rho t = 2.5$ to 100 $\mu g/cm^2$) in the initial phase to determine line shapes and peak locations. As might be expected these thicker targets have a much higher ratio of desirable target x rays versus undesirable contaminent x rays. With thick target ratios as initial values, the fitting process for the thinner targets was expedited. The thick target yields have an estimated uncertainty of ±10%. Due to the buildup of silicon contamination (from diffusion pump oil), the uncertainty in the thinnest target yields was estimated to be ±20%. Combining the efficiency (±6%),

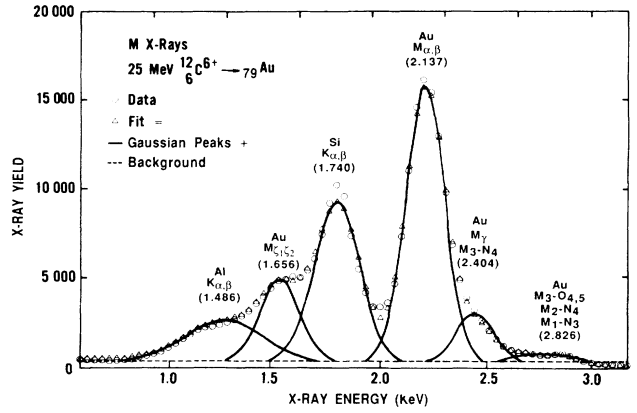

FIG. 1. A typical M-shell spectrum of gold bombarded by 25-MeV carbon ions. The triangles are the fit of six Gaussian peaks (solid curves) plus a linear and nearly constant background (dashed line). These peaks are labeled with the symbol of target atoms (gold plus aluminum and silicon contaminants) and dominant x-ray transitions (with x-ray energies given in keV). Some target transitions ($M_3 \rightarrow N_1$, etc.) are obscured by the contaminents.

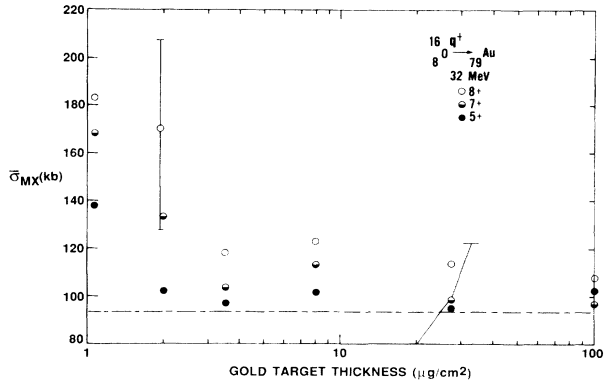

FIG. 2. Enhancement of the effective target M-shell x-ray production cross sections, $\bar{\sigma}_{MX}$, occur with the decreasing thickness of the target and for increasing ion charge state (Ref. 34). The slight rise of the 5+ cross sections (zero K-shell vacancies) is attributed to the relative increase in target contamination as the thickness decreases. The much greater increase for the 7+ (one K vacancy) and the 8+ (two K vacancies) results are due to EC to the projectile K shell. The dashed line represents the cross section for DI plus EC to the $L,M,\ldots$ shells in the ECPSSR formalism. Representative error bars are shown. The filled (●), half-filled (◒), and empty circles (○) of the data correspond to the filled, half-filled, and empty K shell that the projectile brings into the collision.

fluorescence yield (±5%), target thickness (±7%), and x-ray yield uncertainties (±10 or ±20%), the overall uncertainty in the x-ray cross sections is ±15% for $\rho t > 2.5$ $\mu g/cm^2$ and ±23% for $\rho t < 2.5$ $\mu g/cm^2$. To the extent that these thin targets represent single-collision conditions, the cross sections are a good approximation of the cross sections for vanishingly thin targets.

Because the L-shell spectra were much less contaminated with low-atomic-number elements, the uncertainties in the x-ray yields were only ±2% for all targets. The uncertainty in the efficiency of the Si(Li) detector is also better known (±3%) in the L-shell energy region. Combining these values with those for fluorescence yield and target thickness, the overall uncertainty in the L-shell x-ray cross sections is ±10% for all measurements.

III. RESULTS

Effective M-shell x-ray production cross sections as a function of target thickness are plotted in Fig. 2 for different charge state ions.[34] Similar results were obtained for the L-shell spectra. The L-shell data for carbon and oxygen ions for the thinnest targets are presented in Tables I and II, respectively. The M-shell data for carbon and oxygen ions for the thinnest targets are presented in Tables III and IV, respectively. The thickness dependence of the yield must be carefully interpreted because the electron configuration of the projectile inside a solid target is not well understood.[35] Early studies by Hopkins[36] and Groeneveld *et al.*[37] indicated that target x-ray yields, from ions which first passed through the carbon backing of the target foil and had more K-shell vacancies, were considerably enhanced over the target x-ray yields when the beam was incident on the target side of the foil.

This dependence of x-ray yields on projectile charge state and target thickness have also been investigated by Gray *et al*[38] and McDaniel *et al.*[39] They measured target K-shell x-ray yields for projectiles with zero, one, and two K-shell vacancies as a function of target thickness. By varying the number of projectile K-shell vacancies and target thicknesses, they controlled the amount of K-shell to K-shell EC from the target to the projectile. Both groups found that x-ray yields were strongly influenced by the presence of projectile inner-shell vacancies and that the projectile charge state would equilibrate at large target thicknesses. McDaniel *et al.*[39] compared their results favorably with the ECPSSR. McDaniel *et al.*[26] later extended this investigation to the production of L-shell x rays and found similarly good agreement. McDaniel *et al.*[26,39] used the thinnest possible targets (approximately 1 $\mu g/cm^2$), which approximated single-collision conditions, to extract DI and EC cross sections.

The variation of M-shell x-ray production cross sections with projectile inner-shell vacancies has recently been measured[10,32,40] and compared to the first Born and ECPSSR theories. Again it was found that the ECPSSR was in good agreement with the data.

In Figs. 2–6 the filled circles represent target cross sections $\sigma^{(0)}$ for projectiles with no K-shell vacancies, while the half-filled circles and open circles show target cross sections for projectiles with one $\sigma^{(1)}$ and two $\sigma^{(2)}$ K-shell vacancies, respectively. Whereas the $\sigma^{(0)}$ results in Fig. 2 are constant within statistical limits for all but the thinnest targets, the $\sigma^{(1)}$ and $\sigma^{(2)}$ results rise

TABLE I. *L*-shell x-ray production cross sections of several thin targets for incident projectiles of 25 MeV $^{12}_{6}C^{q+}$ ($q = +4,5,6$) (2.08 MeV/amu). From top to bottom, the first three cross sections represent DI + EC for zero, one, and two *K*-shell vacancies in the projectile. The last two groups are the inferred EC cross sections for one and two *K*-shell vacancies. Cross sections are in kilobarns. Uncertainties are ±10% and ±14% for the measured and inferred results, respectively.

	Targets	$_{60}$Nd	$_{64}$Gd	$_{67}$Ho	$_{70}$Yb	$_{79}$Au	$_{82}$Pb
	Z_1/Z_2	0.1	0.094	0.09	0.086	0.076	0.073
Cross	v_1/v_{2L}	0.71	0.64	0.60	0.56	0.47	0.45
sections	ρt (μg/cm^2)	1.4	0.8	0.48	1.35	0.56	1.24
$\sigma_{LX}^{(0)}$	First Born	8.15	5.46	4.11	3.08	1.33	1.00
	ECPSSR	4.18	2.75	2.06	1.55	0.70	0.53
	Expt.	4.95	3.75	2.46	1.97	0.67	0.52
$\sigma_{LX}^{(1)}$	First Born	11.1	6.97	5.04	3.65	1.46	1.08
	ECPSSR	4.77	3.05	2.24	1.66	0.72	0.55
	Expt.	5.65	3.95	2.59	2.08	0.74	0.56
$\sigma_{LX}^{(2)}$	First Born	14.0	8.49	5.98	4.22	1.59	1.16
	ECPSSR	5.36	3.34	2.42	1.76	0.74	0.56
	Expt.	5.70	4.00	2.81	2.12	0.71	0.54
$\sigma_{LX}^{EC(L\to 1/2K)}$	First Born	2.95	1.51	0.93	0.57	0.13	0.08
	ECPSSR	0.59	0.30	0.18	0.11	0.02	0.02
	Expt.	0.70	0.20	0.13	0.11	0.07	0.04
$\sigma_{LX}^{EC(L\to K)}$	First Born	5.85	3.03	1.87	1.14	0.26	0.16
	ECPSSR	1.18	0.59	0.36	0.21	0.04	0.03
	Expt.	0.75	0.25	0.35	0.15	0.04	0.02

significantly in all targets as their thicknesses decrease. The rise in $\sigma^{(0)}$ for the thinnest targets is attributed to the increasing contribution of contaminate x rays from low-atomic-number elements. Assuming a constant amount of contaminant, the associated error will increase as the target of interest gets thinner. The disproportionately large enhancement of $\sigma^{(1)}$ and $\sigma^{(2)}$ reflects the contribution of EC cross sections when the projectiles carry *K* vacancies into the collision and have no chance to equilibrate in the thinnest targets.

The x-ray cross sections for all targets were determined from the results for the thinnest possible targets where approximately single-collision conditions exist. The agreement between the ECPSSR theory and data for the *L* shell is very good (Fig. 3) as compared with the *M*-shell discrepancies (Fig. 4). The *M*-shell data are subject to larger uncertainties than the *L*-shell data because of the greater complexity of their spectra, the contribu-

TABLE II. *L*-shell x-ray production cross sections of several thin targets for incident projectiles of 32 MeV $^{16}_{8}O^{q+}$ ($q = +5,7,8$) (2.00 MeV/amu). From top to bottom, the first three cross sections represent DI + EC for zero, one, and two *K*-shell vacancies in the projectile. The last two groups are the inferred EC cross sections for one and two *K*-shell vacancies. Cross sections are in kilobarns. Uncertainties are ±10% and ±14% for the measured and inferred results, respectively.

	Targets	$_{60}$Nd	$_{64}$Gd	$_{67}$Ho	$_{70}$Yb	$_{79}$Au	$_{82}$Pb
	Z_1/Z_2	0.133	0.125	0.119	0.114	0.101	0.098
Cross	v_1/v_{2L}	0.48	0.45	0.43	0.41	0.36	0.35
sections	ρt (μg/cm^2)	1.4	0.8	0.48	1.35	0.55	1.24
$\sigma_{LX}^{(0)}$	First Born	16.8	10.9	8.06	5.94	2.47	1.85
	ECPSSR	6.42	4.11	3.03	2.25	0.99	0.75
	Expt.	7.25	4.82	3.49	2.83	1.06	0.71
$\sigma_{LX}^{(1)}$	First Born	32.9	19.3	13.2	9.04	3.15	2.25
	ECPSSR	9.10	5.39	3.78	2.69	1.08	0.81
	Expt.	8.56	5.90	3.57	2.99	1.12	0.73
$\sigma_{LX}^{(2)}$	First Born	49.0	27.6	18.3	12.1	3.83	2.65
	ECPSSR	11.8	6.67	4.53	3.13	1.17	0.86
	Expt.	10.45	5.99	3.99	3.21	1.16	0.85
$\sigma_{LX}^{EC(L\to 1/2K)}$	First Born	16.1	8.40	5.14	3.10	0.68	0.40
	ECPSSR	2.68	1.28	0.75	0.44	0.09	0.06
	Expt.	1.31	1.08	0.08	0.16	0.06	0.02
$\sigma_{LX}^{EC(L\to K)}$	First Born	32.2	16.7	10.2	6.16	1.36	0.80
	ECPSSR	5.38	2.56	1.50	0.88	0.18	0.11
	Expt.	3.20	1.17	0.50	0.38	0.10	0.13

TABLE III. M-shell x-ray production cross sections of several thin targets for incident projectiles of 25 MeV $^{12}_{6}C^{q+}$ ($q=+4,5,6$) (2.08 MeV/amu). From top to bottom, the first three cross sections represent DI + EC for zero, one, and two K-shell vacancies in the projectile. The last two groups are the inferred EC cross sections for one and two K-shell vacancies. Cross sections are in kilobarns. Uncertainties are ±23% and ±33% for the measured and inferred results, respectively.

	Targets	$_{60}$Nd	$_{64}$Gd	$_{67}$Ho	$_{70}$Yb	$_{79}$Au	$_{82}$Pb
	Z_1/Z_2	0.1	0.094	0.09	0.086	0.076	0.073
Cross	$v_1/v_{2M4,5}$	0.71	0.64	0.60	0.56	0.47	0.45
sections	ρt (μg/cm^2)	1.4	2.25	0.48	1.35	0.55	1.24
$\sigma_{MX}^{(0)}$	First Born	94.4	123	131	134	87.2	73.4
	ECPSSR	70.5	92.1	97.9	99.1	61.7	51.1
	Expt.	171	78.1	225	177	67.1	87.6
$\sigma_{MX}^{(1)}$	First Born	173	220	232	232	147	123
	ECPSSR	92.7	119	126	127	79.5	65.9
	Expt.	189	92.0	245	181	91.5	99.5
$\sigma_{MX}^{(2)}$	First Born	251	317	332	331	207	173
	ECPSSR	115	146	154	155	97.3	80.8
	Expt.	201	98.6	272	190	93.2	104
$\sigma_{MX}^{EC(M\to 1/2K)}$	First Born	78.6	97.0	101	98.0	59.8	49.6
	ECPSSR	22.2	26.9	28.1	27.9	17.8	14.8
	Expt.	18.0	13.9	20.0	4.0	24.4	11.9
$\sigma_{MX}^{EC(M\to K)}$	First Born	157	194	201	198	120	99.6
	ECPSSR	44.5	53.9	56.1	55.9	35.6	29.7
	Expt.	30.0	20.5	47.0	13.0	26.1	16.4

tion of contaminant x rays, and lesser knowledge of the Si(Li) detector efficiency in the M-shell x-ray energy region.

The first Born (PWBA plus OBKN) theory consistently overpredicts the data for all projectile charge states in Figs. 3 and 4. Again the experimental data are much closer to the ECPSSR than the first Born theory.

The inferred L-shell EC cross sections for one and two K vacancies (Fig. 5) were obtained by subtracting the DI plus EC to $M,N,\ldots$ shells contribution $\sigma_{LX}^{(0)}$ from the total (DI + EC) cross sections $\sigma_{LX}^{(1)}$ and $\sigma_{LX}^{(2)}$ which includes DI plus EC to empty $L,M,N,\ldots$ shells,

$$\sigma_{LX}^{EC[L\to(i/2)K]}=\sigma_{LX}^{(i)}-\sigma_{LX}^{(0)},\quad i=1,2\ .$$

The uncertainty associated with these inferred L- to K-shell EC cross sections is larger than the uncertainties of the original measurements.[41] The EC contribution to the total cross section is generally less than 50%. There-

TABLE IV. M-shell x-ray production cross sections of several thin targets for incident projectiles of 32 MeV $^{16}_{8}O^{q+}$ ($q=+5,7,8$) (2.00 MeV/amu). From top to bottom, the first three cross sections represent DI + EC for zero, one, and two K-shell vacancies in the projectile. The last two groups are the inferred EC cross sections for one and two K-shell vacancies. Cross sections are in kilobarns. Uncertainties are ±23% and ±33% for the measured and inferred results, respectively.

	Targets	$_{60}$Nd	$_{64}$Gd	$_{67}$Ho	$_{70}$Yb	$_{79}$Au	$_{82}$Pb
	Z_1/Z_2	0.133	0.125	0.119	0.114	0.101	0.098
Cross	$v_1/v_{2M4,5}$	0.48	0.45	0.43	0.41	0.36	0.35
sections	ρt (μg/cm^2)	1.4	0.8	0.48	1.35	1.07	1.24
$\sigma_{MX}^{(0)}$	First Born	243	308	325	327	209	175
	ECPSSR	142	183	194	195	120	97.9
	Expt.	288	240	255	201	157	165
$\sigma_{MX}^{(1)}$	First Born	546	723	772	776	488	407
	ECPSSR	230	296	312	313	198	165
	Expt.	341	295	294	234	192	182
$\sigma_{MX}^{(2)}$	First Born	849	1140	1220	1220	768	640
	ECPSSR	317	409	430	431	277	232
	Expt.	417	340	391	278	209	212
$\sigma_{MX}^{EC(M\to 1/2K)}$	First Born	303	415	447	449	279	232
	ECPSSR	88.0	113	118	118	78.0	67.1
	Expt.	53.3	54.2	38.9	32.7	35.1	16.4
$\sigma_{MX}^{EC(M\to K)}$	First Born	606	832	895	893	559	465
	ECPSSR	175	226	236	236	157	134
	Expt.	129	99.3	135	77.4	51.5	46.5

fore a small error in the DI cross section can result in a large error in the inferred L- to K-shell EC cross section. To the extent that the cross sections $\sigma^{(i)}$ are uncorrelated, the uncertainty of the inferred results is the square root of the sum of the squares of the individual uncertainties (i.e., $\pm 14\%$).

As with the L-shell data, the inferred M-shell EC cross sections (Fig. 6) are reported as the difference between the zero K-shell vacancy results $\sigma^{(0)}_{MX}$ and the one $\sigma^{(1)}_{MX}$ and two $\sigma^{(2)}_{MX}$ K-shell vacancy results. Again, the uncertainty of the inferred results ($\pm 33\%$) is greater than the individual uncertainties ($\pm 23\%$). While both theories overestimate the M-shell data, the ECPSSR is closer to the data and the agreement appears to improve with increasing Z_1/Z_2.

In summary the L- and M-shell x-ray production cross sections for 25 MeV ${}^{12}_{6}C^{q+}$ ($q=4,5,6$) and 32 MeV ${}^{16}_{8}O^{q+}$ ($q=5,7,8$) incident upon Nd, Gd, Ho, Yb, Au, and Pb have been measured as a function of target thickness. Measurements made for the thinnest targets (0.48 to 2.25 $\mu g/cm^2$) were used to extract cross sections for DI plus EC to $L,M,\ldots$ shells and electron capture to the K shell. In comparing the L-shell results to the first Born and the ECPSSR theories, it was found that the PWBA plus OBK theory of Nikolaev consistently overpredicted the data by an order of magnitude or more

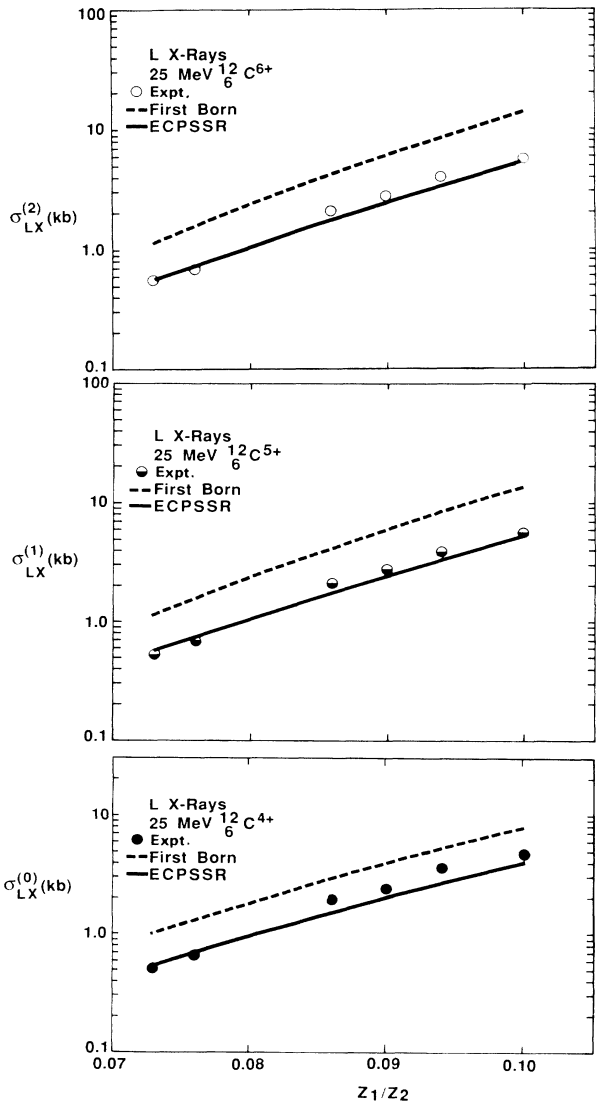

FIG. 3. L-shell x-ray production cross sections by carbon ions. The curves represent the sum of direct ionization plus electron capture from the L shell to the projectile $L,M,\ldots$ shells, $\frac{1}{2}K,L,M,\ldots$ shells, and $K,L,M,\ldots$ shells for $\sigma^{(i)}_{LX}$ $i=0,1,2$, respectively. The absolute uncertainty is $\pm 10\%$ and is approximately the extent of the circular data points.

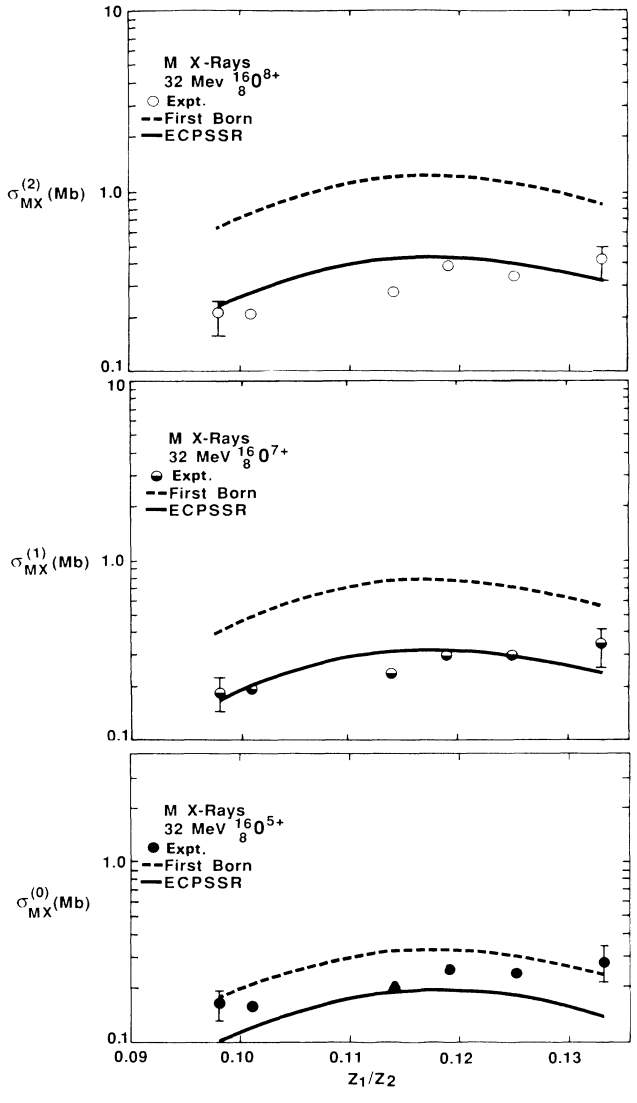

FIG. 4. M-shell x-ray production cross sections by oxygen ions. The curves represent the sum of direct ionization plus electron capture from the M shell to the projectile $L,M,\ldots$ shells, $\frac{1}{2}K,L,M,\ldots$ shells, and $K,L,M,\ldots$ shells for $\sigma^{(i)}_{MX}$ $i=0,1,2$, respectively. The absolute uncertainty is $\pm 23\%$ as shown by the representative error bars.

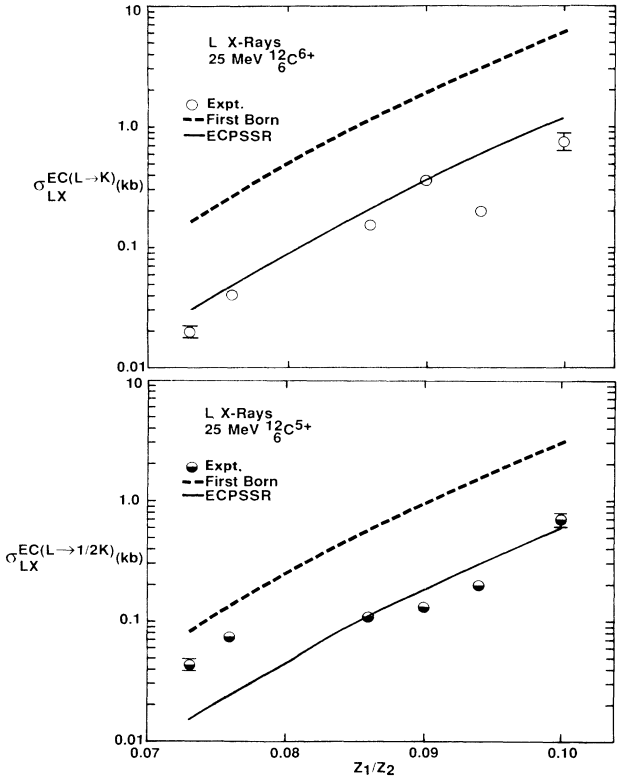

FIG. 5. Inferred L-shell x-ray production cross sections due to EC to the projectile for (◒), a single K-shell vacancy (half-filled circles), and for (○), a double K-shell vacancy (empty circles). The absolute uncertainty is ±14% as shown by the representative error bars.

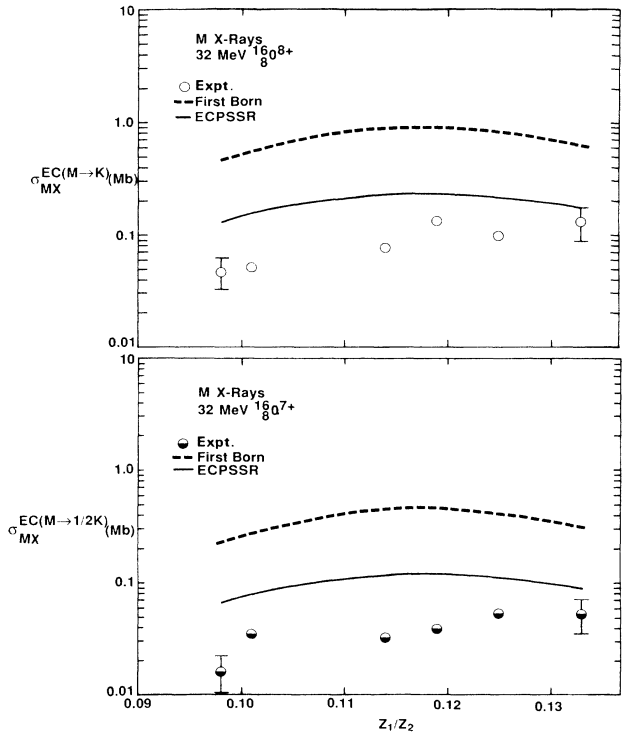

FIG. 6. Inferred M-shell x-ray production cross sections due to EC to the projectile. The (◒), single K-shell vacancies, are represented by half-filled circles and (○), the double K-shell vacancies, are represented by empty circles. The absolute uncertainty is ±33% as shown by the representative error bars.

while the ECPSSR theory was in very good agreement with the data. For the M shell the agreement between either theory and the data was not as good. Nevertheless, the ECPSSR gave better overall agreement

ACKNOWLEDGMENTS

We wish to thank Rand Watson of Texas A&M University for the FACELIFT program. North Texas State University is supported in part by the Robert A. Welch Foundation and the NTSU Organized Research Fund. Research at Oak Ridge National Laboratory was sponsored by the U.S. Department of Energy, Division of Chemical Science, under Contract No. DE-AC05-840R21400 with Martin Marietta Energy Systems, Inc. Additional support is provided by Oak Ridge Associated Universities.

*Present address: Radiation Research Associates, 3815 Lisbon, Ft. Worth, TX 76107.

[1]F. D. McDaniel, Nucl. Instrum. Methods **214**, 57 (1983).
[2]B. M. Johnson, IEEE Trans. Nucl. Sci. **NS-26**, 1312 (1979); B. M. Johnson, K. W. Jones, J. L. Cecchi, and T. H. Kruse, *ibid.* **NS-26**, 1317 (1979).
[3]J. Kliwer and A. ElFiqi, IEEE Trans. Nucl. Sci. **NS-26**, 1323 (1979).
[4]B. D. Sartwell, A. B. Campbell, B. S. Covino, and T. J. Driscoll, IEEE Trans. Nucl. Sci. **NS-26**, 1670 (1979).
[5]K. R. Akselsson, IEEE Trans. Nucl. Sci. **NS-28**, 1370 (1981).
[6]J. D. Spaulding, in *Proceedings of the Second Oak Ridge Conference on the Use of Small Accelerators for Teaching and Research, Oak Ridge, 1970,* edited by J. L. Duggan (Oak Ridge Associated Universities, Oak Ridge, TN, 1970), p. 113 and references therein.
[7]J. M. Khan and D. L. Potter, Phys. Rev. A **133**, 890 (1964).
[8]W. Brandt and G. Lapicki, Phys. Rev. A **20**, 465 (1979), and references therein; J. L. Duggan, P. M. Kocur, J. L. Price, F. D. McDaniel, R. Mehta, and G. Lapicki, *ibid.* **32**, 2088 (1985).
[9]M. C. Andrews, F. D. McDaniel, J. L. Duggan, R. Mehta, G. Lapicki, P. D. Miller, P. L. Pepmiller, H. F. Krause, T. M. Rosseel, and L. A. Rayburn, Nucl. Instrum. Methods B

10/11, 181 (1985), and references therein.
[10]R. Mehta, J. L. Duggan, J. L. Price, F. D. McDaniel, and G. Lapicki, Phys. Rev. A **26**, 1883 (1982).
[11]E. Merzbacher and H. W. Lewis, in *Encyclopedia of Physics*, edited by S. Flugge (Springer-Verlag, Berlin, 1958), Vol. **34**, p. 166.
[12]G. S. Khandelwal, B.-H. Choi, and E. Merzbacher, At. Data **1**, 103 (1969); G. S. Khandelwal and E. Merzbacher, Phys. Rev. **151**, 12 (1970); D. E. Johnson, G. Basbas, and F. D. McDaniel, At. Data Nucl. Data Tables **24**, 1 (1979).
[13]J. D. Garcia, Phys. Rev. A **1**, 280 (1970); **1**, 1402 (1970); **4**, 955 (1971).
[14]J. Bang and J. M. Hansteen, K. Dan. Vidensk. Selsk. Mat. Fys. Medd. **31**(13) (1959); J. M. Hansteen and O. P. Mosebekk, Z. Phys. **234**, 281 (1970); Nucl. Phys. A **201**, 541 (1973).
[15]W. Brandt, R. Laubert, and I. Sellin, Phys. Rev. Lett. **21**, 518 (1966); Phys. Rev. **151**, 56 (1966); W. Brandt and R. Laubert, Phys. Rev. Lett. **24**, 1037 (1970).
[16]G. Basbas, W. Brandt, and R. Laubert, Phys. Rev. A **7**, 983 (1973).
[17]A. M. Halpern and J. Law, Phys. Rev. Lett. **31**, 4 (1973).
[18]J. R. Oppenheimer, Phys. Rev. **31**, 349 (1928); H. C. Brinkman and H. A. Kramers, Proc. Acad. Sci. (Amsterdam) **33**, 973 (1930).
[19]V. S. Nikolaev, Zh. Eskp. Theor. Fiz. **51**, 1263 (1966) [Sov. Phys.—JETP **24**, 847 (1967)].
[20]G. Basbas, W. Brandt, and R. H. Ritchie, Phys. Rev. A **7**, 1971 (1973).
[21]G. Basbas, W. Brandt, and R. Laubert, Phys. Rev. A **17**, 1655 (1978).
[22]G. Lapicki and W. Losonsky, Phys. Rev. A **15**, 896 (1977).
[23]G. Lapicki, IEEE Trans. Nucl. Sci. **NS-28**, 1066 (1981).
[24]W. Brandt and G. Lapicki, Phys. Rev. A **10**, 474 (1974).
[25]G. Lapicki and F. D. McDaniel, Phys. Rev. A **22**, 1896 (1980); A **23**, 975 (1981).
[26]F. D. McDaniel, A. Toten, R. S. Peterson, J. L. Duggan, S. R. Wilson, J. D. Gressett, P. D. Miller, and G. Lapicki, Phys. Rev. A **19**, 1517 (1979).
[27]W. Brandt and G. Lapicki, Phys. Rev. A **23**, 1717 (1981); R. K. Rice, F. D. McDaniel, G. Basbas, and J. L. Duggan, Phys. Rev. A **24**, 758 (1981).
[28]G. Lapicki, Bull. Am. Phys. Soc. **26**, 1310 (1981).
[29]P. M. Kocur, J. L. Duggan, R. Mehta, J. Robbins, and F. D. McDaniel, IEEE Trans. Nucl. Sci. **NS-30**, 1580 (1983).
[30]W. N. Lennard and D. Phillips, Nucl. Instrum. Methods **166**, 521 (1979).
[31]E. J. McGuire, Phys. Rev. A **5**, 1043 (1972).
[32]R. Mehta, J. L. Duggan, F. D. McDaniel, M. C. Andrews, G. Lapicki, P. D. Miller, L. A. Rayburn, and A. R. Zander, Phys. Rev. A **28**, 2722 (1983).
[33]FACELIFT is a least-squares routine which fits several Gaussian peaks plus a linear background simultaneously. It was obtained from R. Watson at the Physics Department, Texas A&M University.
[34]Figure 2 was taken from Ref. 10.
[35]H. D. Betz, Rev. Mod. Phys. **44**, 405 (1972).
[36]F. Hopkins, Phys. Rev. Lett. **35**, 270 (1975).
[37]K. O. Groeneveld, B. Kolb, J. Schader, and K. D. Sevier, Z. Phys. A **277**, 13 (1976); K. O. Groeneveld, B. Kolb, J. Schader, and K. D. Sevier, Nucl. Instrum. Methods **132**, 497 (1976).
[38]T. J. Gray, P. Richard, R. K. Gardner, K. A. Jamison, and J. M. Hall, Phys. Rev. A **14**, 1333 (1976); T. J. Gray, P. Richard, G. Gealy, and J. Newcomb, *ibid.* **19**, 1424 (1979).
[39]F. D. McDaniel, J. L. Duggan, G. Basbas, P. D. Miller, and G. Lapicki, Phys. Rev. A **16**, 1375 (1977).
[40]R. Mehta, J. L. Duggan, J. L. Price, P. M. Kocur, F. D. McDaniel, and G. Lapicki, Phys. Rev. A **28**, 1317 (1983); R. Mehta, *et al.*, IEEE Trans. Nucl. Sci. **NS-30**, 950 (1983); R. Mehta, J. L. Duggan, F. D. McDaniel, M. C. Andrews, G. Lapicki, P. D. Miller, L. A. Rayburn, and A. R. Zander, *ibid.* **NS-30**, 906 (1983).
[41]P. R. Bevington, *Data Reduction and Error Analysis for the Physical Sciences* (McGraw-Hill, New York, 1969).